Down-expression of miR-494-3p in senescent osteocyte-derived exosomes inhibits osteogenesis and accelerates age-related bone loss via PTEN/PI3K/AKT pathway

Correspondence should be
sent to Yafeng Zhang
fcius2004@hotmail.com

C. Yao,[1] J. Sun,[1] W. Luo,[1] H. Chen,[1] T. Chen,[1] C. Chen,[1] B. Zhang,[1] Y. Zhang[1]

Department of Orthopaedics, Affiliated Hospital of Nantong University, Medical School of Nantong University, Nantong, Jiangsu, China

Aims

To investigate the effects of senescent osteocytes on bone homeostasis in the progress of age-related osteoporosis and explore the underlying mechanism.

Methods

In a series of in vitro experiments, we used tert-Butyl hydroperoxide (TBHP) to induce senescence of MLO-Y4 cells successfully, and collected conditioned medium (CM) and senescent MLO-Y4 cell-derived exosomes, which were then applied to MC3T3-E1 cells, separately, to evaluate their effects on osteogenic differentiation. Furthermore, we identified differentially expressed microRNAs (miRNAs) between exosomes from senescent and normal MLO-Y4 cells by high-throughput RNA sequencing. Based on the key miRNAs that were discovered, the underlying mechanism by which senescent osteocytes regulate osteogenic differentiation was explored. Lastly, in the in vivo experiments, the effects of senescent MLO-Y4 cell-derived exosomes on age-related bone loss were evaluated in male SAMP6 mice, which excluded the effects of oestrogen, and the underlying mechanism was confirmed.

Results

The CM and exosomes collected from senescent MLO-Y4 cells inhibited osteogenic differentiation of MC3T3-E1 cells. RNA sequencing detected significantly lower expression of miR-494-3p in senescent MLO-Y4 cell-derived exosomes compared with normal exosomes. The upregulation of exosomal miR-494-3p by miRNA mimics attenuated the effects of senescent MLO-Y4 cell-derived exosomes on osteogenic differentiation. Luciferase reporter assay demonstrated that miR-494-3p targeted phosphatase and tensin homolog (PTEN), which is a negative regulator of the phosphoinositide 3-kinase (PI3K)/AKT pathway. Overexpression of PTEN or inhibition of the PI3K/AKT pathway blocked the functions of exosomal miR-494-3p. In SAMP6 mice, senescent MLO-Y4 cell-derived exosomes accelerated bone loss, which was rescued by upregulation of exosomal miR-494-3p.

Conclusion

Reduced expression of miR-494-3p in senescent osteocyte-derived exosomes inhibits osteogenic differentiation and accelerates age-related bone loss via PTEN/PI3K/AKT pathway.

Article focus

- Effects of senescent osteocytes on bone homeostasis in age-related osteoporosis and the underlying mechanism.

Key messages

- Senescent osteocyte-derived exosomes inhibit osteogenic differentiation and accelerate age-related bone loss.

Bone & Joint Research

- The expression of miR-494-3p in senescent osteocyte-derived exosomes is reduced, which mediates the effects of these exosomes via the phosphatase and tensin homolog (PTEN)/phosphoinositide 3-kinase (PI3K)/AKT pathway.

Strengths and limitations

- This study revealed for the first time the phenomenon and mechanism of senescent osteocyte-derived exosomes influencing bone homeostasis, providing a novel therapeutic strategy for age-related osteoporosis.
- The effects of senescent osteocytes on the function of osteoclasts and bone resorption were not investigated in this study and warrant further research.

Introduction

Age-related osteoporosis is one of the most common degenerative diseases worldwide with the continued ageing of the global population.[1] It is characterized by decreased bone mass and disrupted bone microarchitecture, which causes a higher incidence of fragility fractures, low back pain, and other complications.[2,3] Unfortunately, the currently available therapies, including treatment with an antiresorptive modulator, calcitonin, bisphosphonates, vitamin D, and some other drugs, cannot reverse the trend of bone loss and typically cause adverse side effects.[4-6] Due to the high mortality, disability rate, morbidity, and socioeconomic burden associated with age-related osteoporosis or fragility fractures,[7,8] a clear understanding of the underlying pathogenic mechanism is urgently needed to facilitate the development of effective therapies for this disease.

Normally, the processes of bone formation by osteoblasts and bone resorption by osteoclasts are coupled tightly. As old bone is replaced with new bone, the dynamic balance maintained within healthy bone tissue is called 'bone homeostasis', and many skeletal diseases occur due to the disruption of bone homeostasis.[9,10] In age-related osteoporosis, the bone turnover rate is slower, which mainly manifests as decreased bone formation.[11] Osteoblast function weakens with ageing, and limited bone formation or mineralization cannot fill the resorption cavity left by osteoclasts, resulting in bone mass loss and bone microarchitecture disorder. This process is known to be influenced by several factors, including the cellular microenvironment, hormone levels, inflammation, vascularization, oxidative stress, etc,[12-15] but the major regulators have yet to be determined.

Just like proliferation, differentiation, and apoptosis, senescence is an irreversible cell fate accompanied by enhanced expression of biomarkers such as P16Ink4a and γH2AX. Research has shown that in multiple degenerative diseases, such as atherosclerosis, osteoarthritis, Alzheimer's disease, and Parkinson's disease, senescent cells accumulate in pathological tissues, and the senescence-associated secretory phenotype (SASP) causes tissue dysfunction.[16-18] Targeting cell senescence has been an important strategy for these degenerative diseases.[19,20] Similarly, senescent cells are observed in the bone tissue of old mice, and senescent osteocytes are the major cell type responsible for SASP.[21,22] As they account for more than 90% of all cells in bone, osteocytes have become a main focus of

research related to metabolic skeletal diseases.[23,24] Changes in osteocytes and their regulatory functions related to osteoblasts, osteoclasts, and bone marrow-derived mesenchymal stem cells (BMSCs) during disease progression have been investigated.[25-27] Inhibition of cellular senescence, especially osteocyte senescence, represents a new therapeutic paradigm for age-related osteoporosis. Researchers have proven that specific clearing of senescent osteocytes by genetic or pharmacological approaches can prevent age-related bone loss in mice.[28,29] These findings suggest that the senescent osteocytes may disrupt bone formation and play a causal role in age-related osteoporosis.

Maintenance of bone homeostasis relies on close interaction among osteocytes, osteoblasts, osteoclasts, and other cell types. For example, in the process of bone remodelling, apoptotic osteocytes release signalling molecules to activate differentiation of osteoblasts and osteoclasts.[25,30] Thus, therapies that influence the activities of bone cells by regulating intercellular communication are promising. In addition to direct interaction through molecule exchange, compelling evidence indicates that exosomes play an essential role in cell–cell crosstalk, and the release and uptake of exosomes by different types of bone cells have been documented.[31] The specific components, including proteins, lipids, nucleic acids, and other molecules, transferred through exosomes form a complex network that can mediate the regulation of bone homeostasis and influence osteoporosis progression. Thus, modification of exosomal contents offers a potential approach to prevent or reverse osteoporosis.[32] Compared to the exosomes derived from osteoblasts, osteoclasts, or mesenchymal stem cells,[33,34] research regarding the contents and effects of osteocyte-derived exosomes has been limited, with the first report on osteocyte-derived exosomes and the ability of microRNA (miRNA) within these exosomes to regulate bone homeostasis published in 2017.[35,36]

In the present study, we tested the hypothesis that senescent osteocytes accumulating in bone tissues disrupt bone homeostasis through exosomal factors, thereby accelerating age-related bone loss. We induced senescence in MLO-Y4 cells through induction of oxidative stress, extracted exosomes from these cells, and verified that they inhibit osteogenic differentiation of MC3T3-E1 cells. Significantly lower expression of one miRNA, miR-494-3p, in exosomes of senescent versus normal MLO-Y4 cells was detected through high-throughput RNA sequencing, and further analyses demonstrated that miR-494-3p targets phosphatase and tensin homolog (PTEN), indicating that the effect of exosomal miR-494-3p on osteogenic differentiation and age-related bone loss is mediated via the PTEN/phosphoinositide 3-kinase (PI3K)/Akt pathway.

Methods

Cell culture

The MLO-Y4 mouse osteocyte cell line and MC3T3-E1 mouse embryo osteoblast precursor cell line (subclone 14) were obtained from China's National Collection of Authenticated Cell Cultures and routinely cultured in α-modified Eagle's Minimum Essential Medium (α-MEM)

Down-expression of miR-494-3p in senescent osteocyte-derived exosomes inhibits osteogenesis and accelerates age-related bone loss via PTEN/PI3K/AKT pathway
C. Yao, J. Sun, W. Luo, et al

53

supplemented with 10% (v/v) fetal bovine serum (Gibco, Life Technologies; Thermo Fisher Scientific, USA) and penicillin/streptomycin (pen/strep, 100 U/ml and 100 μg/ml; Gibco) at 37℃ in 5% CO_2.

In vitro model of cell senescence

Tert-butyl hydroperoxide (TBHP) was used to establish the senescence model of bone cells in vitro. Briefly, MLO-Y4 cells were treated with different concentrations (0, 12.5, 25, or 37.5 μM) of TBHP by directly adding the respective volume of TBHP (diluted in α-MEM) to the media followed by incubation for different lengths of time (0, 12, 24, or 48 hrs). Senescence-associated β-galactosidase (SA-β-Gal) staining and testing for γH2AX and P16 by western blotting or immunofluorescence staining confirmed the success of senescence induction of MLO-Y4 cells. The Cell Counting Kit 8 (CCK-8) assay (Dojindo, Japan) was used to determine the optimal concentration and time of the TBHP treatment (25 μM, 24 hrs). We obtained control conditioned medium (CM) from non-treated MLO-Y4 cell cultures and CM from senescent MLO-Y4 cells treated with 25 μM THBP for 24 hours.

CCK-8 assay

Cell viability was tested by using the CCK-8 assay. MLO-Y4 cells or MC3T3-E1 cells were seeded into 96-well plates (1.5 × 10^4 cells/cm²), and blank wells did not contain cells. At the specified detection timepoint, the cells in each well were treated with 10 μl CCK-8 solution and incubated at 37℃ for one hour. The absorbance of the solution in each well was measured at 450 nm, and the survival/proliferation of the cells was calculated by subtracting the optical density (OD) of the blank well from the OD of the cell-containing wells. The CCK8 assay results were used to determine the optimal concentration and time of drug or exosome treatment of cells.

SA-β-Gal staining

SA-β-Gal staining was performed using a Senescent Cell β-Galactosidase Staining Kit (G1073; Servicebio, China) according to the manufacturer's protocol. Briefly, MLO-Y4 cells were washed three times with phosphate-buffered saline (PBS) and then fixed with 2% paraformaldehyde (PFA) and 0.2% glutaraldehyde for 15 minutes. Next, fixed MLO-Y4 cells were incubated in SA-β-Gal staining solution at 37℃ for eight to 24 hours. Stained MLO-Y4 cells were imaged on an inverted fluorescence microscope (IX73; Olympus, Japan). Total MLO-Y4 cells and SA-β-Gal–positive MLO-Y4 cells were counted in three random fields per dish.

γH2AX and P16 immunofluorescence staining

MLO-Y4 cells were seeded on glass cover slips for immunofluorescence experiments and fixed in 4% PFA. The cells were permeabilized in PBS containing 0.1% sodium citrate and 0.3% Triton-X, and blocking was performed by addition of 1% bovine serum albumin (BSA) in PBS. The cells were incubated in solutions of γH2AX and P16 antibody (1:1,000; Cell Signaling Technology, USA) overnight at 4℃. Alexa Fluor anti-rabbit 488 and anti-mouse 594 (1:5,000; Cell Signaling Technology) were used as secondary antibodies. Nuclei were counterstained with 4′,6-diamidino-2-phenylindole (DAPI; Sangon Biotech,

China), and the cells were evaluated by fluorescence microscopy (Leica, Germany).

Alkaline phosphatase and Alizarin Red S staining for mineralization

MC3T3-E1 cells were seeded in six-well plates (5 × 10^3 cells/cm²) and cultured in osteogenic induction medium with stimulation for 14 days. To induce osteogenic differentiation, 50 μg/ml L-ascorbic acid (MilliporeSigma, USA), 10 mM β-glycerophosphate (MilliporeSigma), and 10 nM dexamethasone (MilliporeSigma) were added in α-MEM. Alkaline phosphatase (ALP) staining was performed with a nitro-blue tetrazolium/5-bromo-4-chloro-3-indolylphosphate (BCIP/NBT) ALP colour development kit (C3206; Beyotime, China) according to the manufacturer's instructions. Alizarin Red S staining was performed to detect calcium deposits using a modified Alizarin Red S stain kit for calcium (G3280; Solarbio, China). Stained plates were photographed using a digital camera. Images of stained cells were captured under a light microscope (BX41; Olympus), and five randomly selected fields (× 10 magnification) were photographed in each well for analysis using ImageJ software (version 1.53 n; National Institutes of Health, USA).

Western blotting

MC3T3-E1 cells were lysed in lysis buffer (P0013; Beyotime) at 4℃ with protease and phosphatase inhibitors (P1045; Beyotime) 48 hours after stimulation. The lysis mixture was centrifuged at 12,000× rpm for 20 minutes at 4℃, and the supernatant containing cellular proteins was used in the following experiments. The total protein concentration was measured by the Bicinchoninic Acid Protein Assay Kit (Bio-Rad, USA) according to the manufacturer's protocol. Equal amounts (100 μg) of protein were denatured, separated on 8% to 12% sodium dodecyl sulphate-polyacrylamide gel electrophoresis (SDS-PAGE) gels, and transferred to polyvinylidene difluoride (PVDF) membranes (MilliporeSigma). The membranes were blocked with 5% BSA for two hours at room temperature and then incubated with primary antibodies at 4℃ overnight. Next, membranes were incubated with horseradish peroxidase-conjugated secondary antibodies (Cell Signaling Technology) for 1.5 hours at room temperature. The primary antibodies used were P16 (1:1000, ab51243; Abcam, USA), Runt-related transcription factor 2 (Runx2, 1:1,000, 12,556 S; Cell Signaling Technology), collagen type I α1 (Col-I, 1:1,000, 72,026 T; Cell Signaling Technology), ALP antibody (1:1,000, AF2910; R&D Systems, USA), AKT (1:1,000, 60203-2-Ig; Proteintech, USA), phosphorylated (p)-AKT (1:1,000, 66444-1-Ig; Proteintech), PI3K (1:1,000, 20584-1-AP; Proteintech), PTEN (1:1,000, 22034-1-AP; Proteintech), CD9 (1:1,000, 60232-1-Ig; Proteintech), and CD63 (1:1,000, 67605-1-Ig; Proteintech), while glyceraldehyde-3-phosphate dehydrogenase (GAPDH) antibody (1:5,000, 60004-1-Ig; Proteintech) was used as a loading control. The signals were visualized with an enhanced chemiluminescence (ECL) detection reagent (P0018FM; Beyotime) and semi-quantified with ImageJ software (version 1.53 n).

Reverse transcription-quantitative polymerase chain reaction

Total cellular RNA was isolated using an RNA Isolation Kit (R0026; Beyotime) according to the manufacturer's protocol. The RNA concentration was determined by Nanodrop One (Thermo Fisher Scientific). Complementary DNA (cDNA) synthesis was performed from each 1 mg RNA using Swe-Script RT II Enzyme Mix (G3330; Servicebio) following the manufacturer's instructions. Reverse transcription-quantitative polymerase chain reaction (RT-qPCR) for messenger RNA (mRNA) was performed on a LightCycler 480 (Roche Diagnostics, USA) with 2 Universal SYBR Green Fast qPCR Mix (RK21203; ABclonal, USA). *Gapdh* was used as an internal standard control. The following primer sequences were used: *Col1* gene: 5′-TTCTCCTGGCAAAGACGGAC-3′ and 5′-CGGCCACCATCTTGAGACTT-3′; *Runx2* gene: 5′-ATCCCCATCCATCCACTCCA-3′ and 5′-GCCAGAGGCAGAAGTCAGAG-3′; *Alpl* gene: 5′-TAACACCAACGCTCAGGTCC-3′ and 5′-TGGATGTGACCTCATTGCCC-3′; *Pten* gene: 5′-CCTGCAGAAAGACTTGAAGGTG-3′ and 5′-AGCTGTGGTGGGTTATGGTC-3′; *PI3K* gene: 5′-TGTACACCACGGTTTGGACT-3′ and 5′-GGCTACAGTAGTGGGCTTGG-3′; *Akt* gene: 5′-CCGCCTGATCAAGTTCTCCT-3′ and 5′-GATGATCCATGCGGGGCTT-3′; miR-494-3p mimic negative control (NC) gene: 5′-UUCUCCGAACGUGUCACGUTT-3′; mmu-miR-494-3p mimic gene: 5′-UUGUACAUGGUAGGCUUUC-3′; and *Gapdh* gene: 5′-GGAGAGTGTTTCCTCGTCCC-3′ and 5′-ATGAAGGGGTCGTTGATGGC-3′. Bulge-loop miRNA qRT-PCR Primer Sets (one RT primer and a pair of qPCR primers for each set) specific for miR-494-3p, miR-1193-3p, miR-149-3p, miR-184-5p, miR-30a-5p, and miR-770-5p were designed by RiboBio (China).

Collection and identification of exosomes in vitro

Cultures of non-treated and TBHP-treated MLO-Y4 cells were switched to serum-free MEM when the cells reached 80% confluency, and after 24 hours the supernatant was collected, which contained exosomes. The exosomes were then isolated via differential centrifugation (300× g for 10 mins, 1000× g for 10 mins, and 16,500× g for 30 mins) at 4℃ followed by filtration through a 0.2 μm filter (Millicell, Germany), and then two additional rounds of ultracentrifugation (100,000× g for 90 mins) at 4℃. After evaluation by transmission electron microscopy (TEM) and nanoparticle tracking analysis (NTA), the total protein content of the exosomes was measured using a BCA kit (Beyotime), and western blot analysis was performed with antibodies against CD9 (anti-rabbit; MilliporeSigma) and CD63 (anti-mouse; Santa Cruz Biotechnology, USA).

Measurement of exosome uptake

Cellular uptake of exosomes from non-treated and TBHP-treated MLO-Y4 cells was analyzed using a cellular uptake assay employing the PKH-26 labelling kit (MilliporeSigma). At room temperature, resuspended exosome pellets were incubated with PKH-26 dye (4 μl) diluted in Diluent C (300 μl) for five minutes, and the resulting solution was then mixed with FBS (3 ml) and centrifuged at 100,000× g to obtain a pellet of exosomes labelled with PKH-26. Next, MC3T3-E1 cells were incubated in medium containing the labelled exosomes for two hours before being fixed in 4% PFA for 30 minutes at room temperature. The cell nuclei were stained with DAPI,

and exosome uptake within MC3T3-E1 cells was evaluated by fluorescence microscopy (Leica).

Transcriptome sequencing

RNA was extracted from exosomes secreted by control non-treated or TBHP-treated MLO-Y4 cells using Trizol (Life Technologies, UK), and transcriptome sequencing data (mRNA) were acquired using the HiSeq 2500 platform (Illumina, USA). Differentially expressed genes (DEGs) were identified based on absolute value of log2 fold change ≥ 0.5 along with p < 0.05. The biological functions of identified DEGs were investigated by Rhy, Gene Ontology (GO), and Kyoto Encyclopedia of Gene and Genomes (KEGG) pathway analyses (p < 0.01). The p-value threshold set in investigation of identified DEG biological functions represents the correlation between the screened signal pathway and the target gene. TargetScan was also used to identify potential targets of miR-494-3p and PTEN, and the results were further verified by RT-qPCR.

Cell transfection

miRNA-494-3p mimics and the corresponding negative controls (mimic NC) were obtained from GenePharma (China). Lipofectamine 2000 reagent was used for cell transfection. Four groups of MLO-Y4 cells were established for exosome collection: Group 1, control cells, no TBHP or miRNA treatment; Group 2, treatment with 25 μM TBHP only; Group 3, treatment with 25 μM TBHP + miR-494-3p NC; and Group 4, treatment with 25 μM TBHP + miR-494-3p mimics. After 24 hours, the exosomes released by cells in the different groups were collected, and the expression of exosomal miR-494-3p was evaluated by RT-qPCR.

To investigate the role of the miR-494-3p/PTEN/PI3K pathway, five groups of MLO-Y4 cells were established for exosome collection: Group 1, control cells, no TBHP or miRNA treatment; Group 2, treatment with 25 μM TBHP only; Group 3, treatment with 25 μM TBHP + miR-494-3p mimics; Group 4, treatment with 25 μM TBHP + miR-494-3p mimics + PTEN overexpression; and Group 5, treatment with 25 μM TBHP + miR-494-3p mimics + LY294002. Then, exosomes derived from MLO-Y4 cells that had been exposed to different treatments were collected and added to MC3T3-E1 cells, and changes in the activities of MC3T3-E1 cells were assessed by Alizarin Red S staining, ALP staining, western blotting, and RT-qPCR.

Mouse model

Healthy rapidly ageing senescence-accelerated mouse P6 (SAMP6) mice (n = 24), weighing a mean 20 g (standard deviation (SD) 2) and aged four months, were housed under specific pathogen-free (SPF) conditions and maintained under standard laboratory conditions (temperature, 25℃ ± 2; humidity, 50% ± 5), with a 12 hr:12 hr light/dark cycle. To exclude the effects of oestrogen to bone loss, we used male mice in our in vivo experiments. All mice were fed standard rat chow and water ad libitum. After one week of adaptive feeding, all the mice were numbered and divided into four groups in accordance with a random number table (n = 6/group): 1) control group, tail vein injection of 100 μl PBS once per week; 2) control-exosome group, tail vein injection of 100 ng exosomes from control cells dissolved in 100 μl PBS once per week; 3) TBHP-exos group, tail vein injection of 100 ng exosomes from TBHP-treated cells dissolved in

Down-expression of miR-494-3p in senescent osteocyte-derived exosomes inhibits osteogenesis and accelerates age-related bone loss via PTEN/PI3K/AKT pathway
C. Yao, J. Sun, W. Luo, et al

55

100 μl PBS once per week; and 4) TBHP + miR-494-3p mimics-exos group, tail vein injection of 100 ng TBHP + exosomes from cell treated with miR-494-3p mimics dissolved in 100 μl PBS once per week. The entire procedure was repeated for eight weeks. After that, right femora were harvested from the different groups of rats for micro-CT testing. The left femora were harvested from the different groups of rats and fixed in 4% PFA for 48 hours at room temperature before being decalcified for four weeks. Afterwards, 5 μm sections were cut on a paraffin slicing machine for different staining. One-way analysis of variance (ANOVA) among four groups of samples was performed in in vivo experiments, and we determined the sample size according to the degree of freedom (df) of ANOVA. Normally, the df should be 10 to 20 to assure the reliability of ANOVA and avoid wasting experimental resources. In this study, we divided 24 mice into four groups with six mice per group, and the df was 20, which was reasonable for ANOVA. This study was reported in accordance with the ARRIVE guidelines.

Micro-CT scanning and analysis

Micro-CT (SkyScan-1276 microcomputed tomography system; Bruker Micro-CT, Belgium) was used to verify the osteoporotic condition of bones in the mouse model. The right femora were collected and stored at -80℃ before CT scanning. Samples were scanned at 15 μm pixel resolution (1 mm aluminium filter, 85 kV, 200 μA). A total of 135 images were obtained from the distal region of each femur. The femora were visualized along the sagittal and transverse planes by SkyScan CTVox software (Bruker, Germany). Morphological parameters were evaluated using CTAn software (Bruker), including the percentage bone volume (BV) calculated as BV/total volume (TV), bone mineral density (BMD), trabecular number (Tb.N), trabecular thickness (Tb.Th), and trabecular separation (Tb.Sp).

Immunohistochemical staining

As described above, 5 μm sections of harvested bone samples were cut on a paraffin slicing machine and rehydrated to conduct immunohistochemical analysis. After blocking, the slides were incubated overnight at 4℃ with antibody (PI3K, 1:200, 20584-1-AP, Proteintech; PTEN, 1:200, 22034-1-AP, Proteintech; ALP, 1:200, AF2910, R&D Systems; Runx2, 1:200, ab192256, Abcam; Col-I, 1:200, 72,026 T, Cell Signaling Technology) separately. Then the slides were further incubated with secondary antibody at 37℃ for two hours. Finally, the slides were treated with 3,3-diaminobenzidine (DAB, MilliporeSigma) and counterstained with haematoxylin before being sealed and observed with a microscope (Leica).

Immunofluorescence observation of exosomes in vivo

Normal mice received a tail vein injection of 100 ng exosomes from TBHP-treated cells (PKH-26 loaded) dissolved in 100 μl PBS. Harvested bone tissues were sectioned, and the sections were then blocked with blocking reagent containing 0.3% Triton X-100 for 1.5 hours. After washing, the slides were stained with DAPI and observed under a microscope (Leica).

Statistical analysis

There were three replicates for each in vitro experiment and six animals in each group for in vivo experiments. During the whole procedure of experiments and analysis, the specific group allocation of mice, cells, and samples was conducted blind by researchers to reduce the bias of results. Data are expressed as means (SD). Independent-samples t-test was performed for data from two groups. For data from three or more groups, if the variance was uneven, log conversion or non-parametric testing was performed. If the variance satisfied homogeneity, one-way analysis of variance (ANOVA) with Sidak's multiple comparison tests was applied. To test for statistical significance, comparisons between any pair of groups were made with Fisher's least significant difference (LSD) test. In all tests, p-values less than 0.05 were considered to reflect statistical significance.

Results

Senescence induction in MLO-Y4 cells

The application of oxidative stress is an important method for inducing cell senescence. We first induced senescence in murine osteocyte-like MLO-Y4 cells by treatment with TBHP, an external stimulant of oxidative stress, at different concentrations (0, 12.5, 25, or 37.5 μM) and for different lengths of time (0, 12, 24, or 48 hrs). CCK-8 assay showed that cell proliferation decreased after TBHP exposure (Supplementary Figures aa and ab), and SA-β-Gal staining showed that TBHP successfully induced senescence of MLO-Y4 cells in both a time- and concentration-dependent manner (Supplementary Figures ac and ad). We chose 25 μM TBHP and 24 hours as the most appropriate concentration and time for inducing senescence in the next experiments. Furthermore, western blotting, RT-qPCR, and fluorescence staining showed that expression levels of p16 and γH2AX, two classic senescence markers, were increased in MLO-Y4 cells after treatment with 25 μM TBHP for 24 hours (Supplementary Figures ae to ah).

Effects of CM from senescent MLO-Y4 cells on osteogenic differentiation of MC3T3-E1 cells

After senescent MLO-Y4 cells were cultured for 24 hours, we collected the supernatant as CM containing products of senescent MLO-Y4 cells. Supernatant collected from normal MLO-Y4 cells served as the control CM. MC3T3-E1 cells were cultured in osteogenic differentiation medium supplemented with 20% senescent CM or 20% control CM. ALP and Alizarin Red S staining were performed to evaluate the osteogenic differentiation on days 7, 14, and 21. The results showed significantly less staining in the senescence CM group than in the control CM group (Supplementary Figure ba). Similarly, western blotting and RT-qPCR showed that the expression of ALP, Runx2, and Col-I, three osteoblast markers, was significantly lower in the senescent CM group than in the control CM group (Supplementary Figures bb and bc, Supplementary Figure c). These experiments indicated that the senescent MLO-Y4 cells' CM inhibited osteogenic differentiation.

Characteristics of exosomes derived from normal and senescent MLO-Y4 cells

To test our hypothesis that exosomes mediate the effect of senescent osteocytes on osteogenic differentiation, we isolated exosomes from the supernatant of normal and senescent MLO-Y4 cells. TEM showed that the exosomes from both cell groups had intact membranes and typical
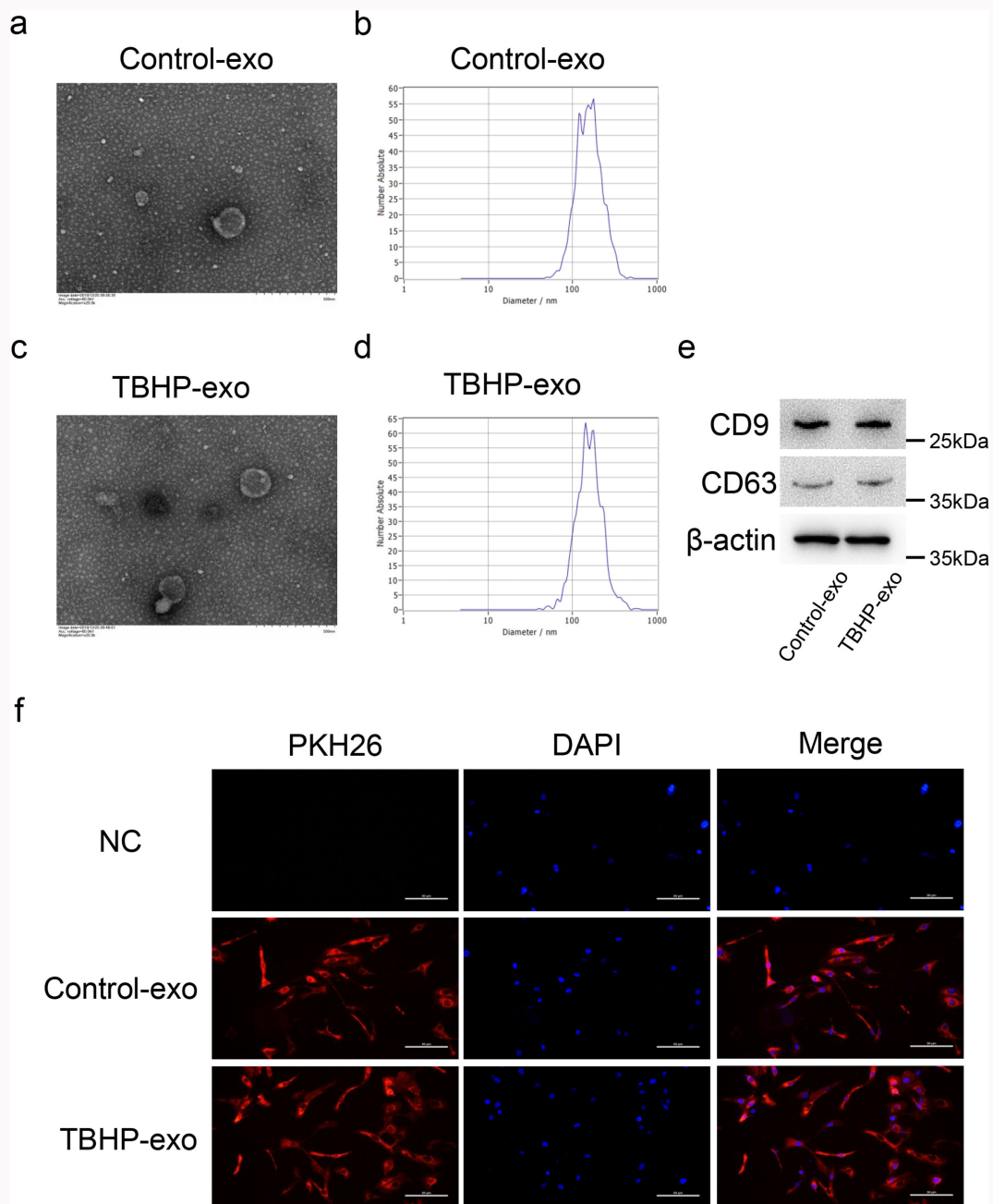
Fig. 1
Characteristics of exosomes derived from normal or senescent MLO-Y4 cells. a) and b) Transmission electron microscopy (TEM) and nanoparticle tracking analysis (NTA) of exosomes derived from normal MLO-Y4 cells. Scale bar = 50 nm. c) and d) TEM and NTA of exosomes derived from senescent MLO-Y4 cells. Scale bar = 50 nm. e) Western blotting of CD9 and CD63 in exosomes derived from normal or senescent MLO-Y4 cells. f) Fluorescence imaging of MC3T3-E1 cells co-cultured with labelled exosomes derived from normal or senescent MLO-Y4 cells for two hours. Red represents exosomes. Blue represents cell nuclei. Scale bar = 50 μm and the magnification is 10×. DAPI, 4, 6-diamidino-2-phenylindole; NC, negative control; TBHP, tert-Butyl hydroperoxide.

cup-shaped morphology (Figure 1c). NTA showed that the exosome size was 150 nm ± 12 (Figure 1d), which was consistent with the size observed by TEM. Two protein markers of exosomes, CD9 and CD63, were detected in exosomes derived from both control and senescent MLO-Y4 cells (Figure 1e). To evaluate exosome endocytosis, we used PKH26 to label the exosomes and added them to cultures of MC3T3-E1 cells for 24 hours. Cell fluorescence imaging showed that MC3T3-E1 cells internalized many exosomes, which suggested that exosomes may deliver their contents from osteocytes to osteoblasts (Figure 1f).

Effects of senescent MLO-Y4 cell-derived exosomes on osteogenic differentiation of MC3T3-E1 cells
MC3T3-E1 cells in osteogenic differentiation medium were treated with different concentrations (20, 100, or 300 μg/ml) of exosomes obtained from TBHP-treated MLO-Y4 cells for different lengths of time (0, 24, 48, or 72 hrs). CCK-8 assay (Figure 2a) showed that 48 hours was the most appropriate time for the following experiments. Then MC3T3-E1 cells in osteogenic differentiation medium were treated with exosomes obtained from normal or TBHP-treated MLO-Y4 cells. ALP and Alizarin Red S staining were performed to
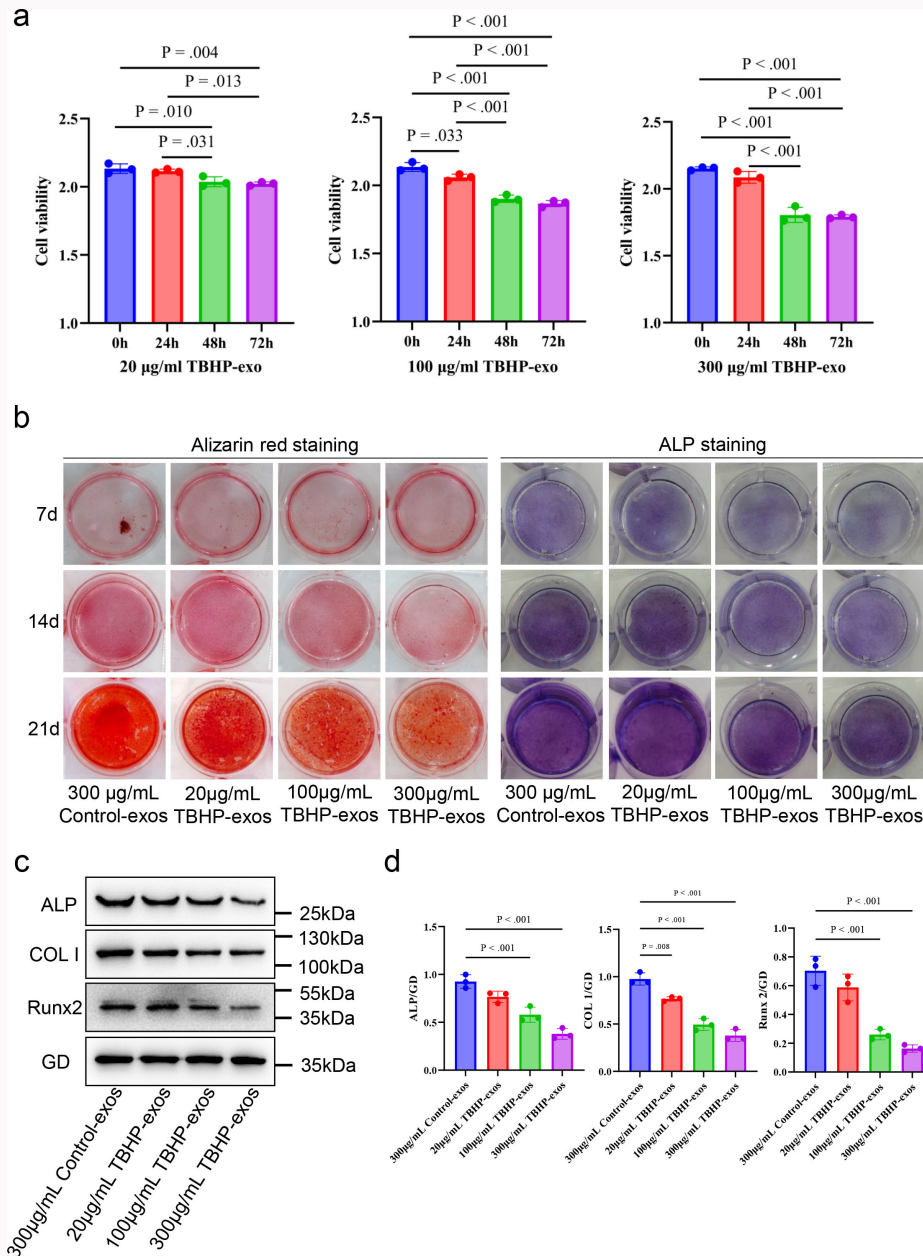
Down-expression of miR-494-3p in senescent osteocyte-derived exosomes inhibits osteogenesis and accelerates age-related bone loss via PTEN/PI3K/AKT pathway
C. Yao, J. Sun, W. Luo, et al

57

Fig. 2
Effects of senescent MLO-Y4 cell-derived exosomes (abbreviated tert-Butyl hydroperoxide (TBHP)-exos in the figure) on osteogenic differentiation of MC3T3-E1 cells. a) Cell Counting Kit 8 (CCK-8) assay of MC3T3-E1 cells treated with different concentrations (20, 100, or 300 μg/ml) of senescent MLO-Y4 cell-derived exosomes for different lengths of time (0, 24, 48, or 72 hours). b) Alkaline phosphatase (ALP) and Alizarin Red S staining of MC3T3-E1 cells on days 7, 14, and 21 after treatment with the indicated concentrations of exosomes obtained from senescent MLO-Y4 cells. c) and d) Western blotting and grayscale analysis of ALP, Runt-related transcription factor 2 (Runx2), and collagen type I α1 (Col-I) expression in MC3T3-E1 cells in different treatment groups. Data are shown as column charts and the p-values were calculated by one-way analysis of variance with Sidak's multiple comparison tests. The p-values were specified only when $p < 0.05$ (statistically significant). GD, glyceraldehyde 3-phosphate dehydrogenase.

evaluate the osteogenic differentiation on days 7, 14, and 21 (Figure 2b), and western blotting and RT-qPCR were performed to measure the ALP, Runx2, and Col-I protein and gene expression levels, respectively (Figure 2d, Supplementary Figure d). The results consistently indicated that the senescent MLO-Y4 cell-derived exosomes inhibited osteogenic differentiation of MC3T3-E1 cells compared with control MLO-Y4 cell-derived exosomes.

Senescent MLO-Y4 cell-derived exosomes inhibit osteogenic differentiation due to reduced expression of exosomal miR-494-3p
To explore the molecular mechanism by which senescent MLO-Y4 cell-derived exosomes inhibit osteogenic differentiation, we performed high-throughput RNA sequencing to compare the miRNA expression profiles of exosomes derived from normal control and senescent MLO-Y4 cells. The results identified 15 miRNAs that were downregulated and 35 miRNAs that were upregulated in senescent MLO-Y4 cell-derived exosomes (Supplementary Figures ea and eb). GO enrichment analysis showed that the differentially expressed miRNAs
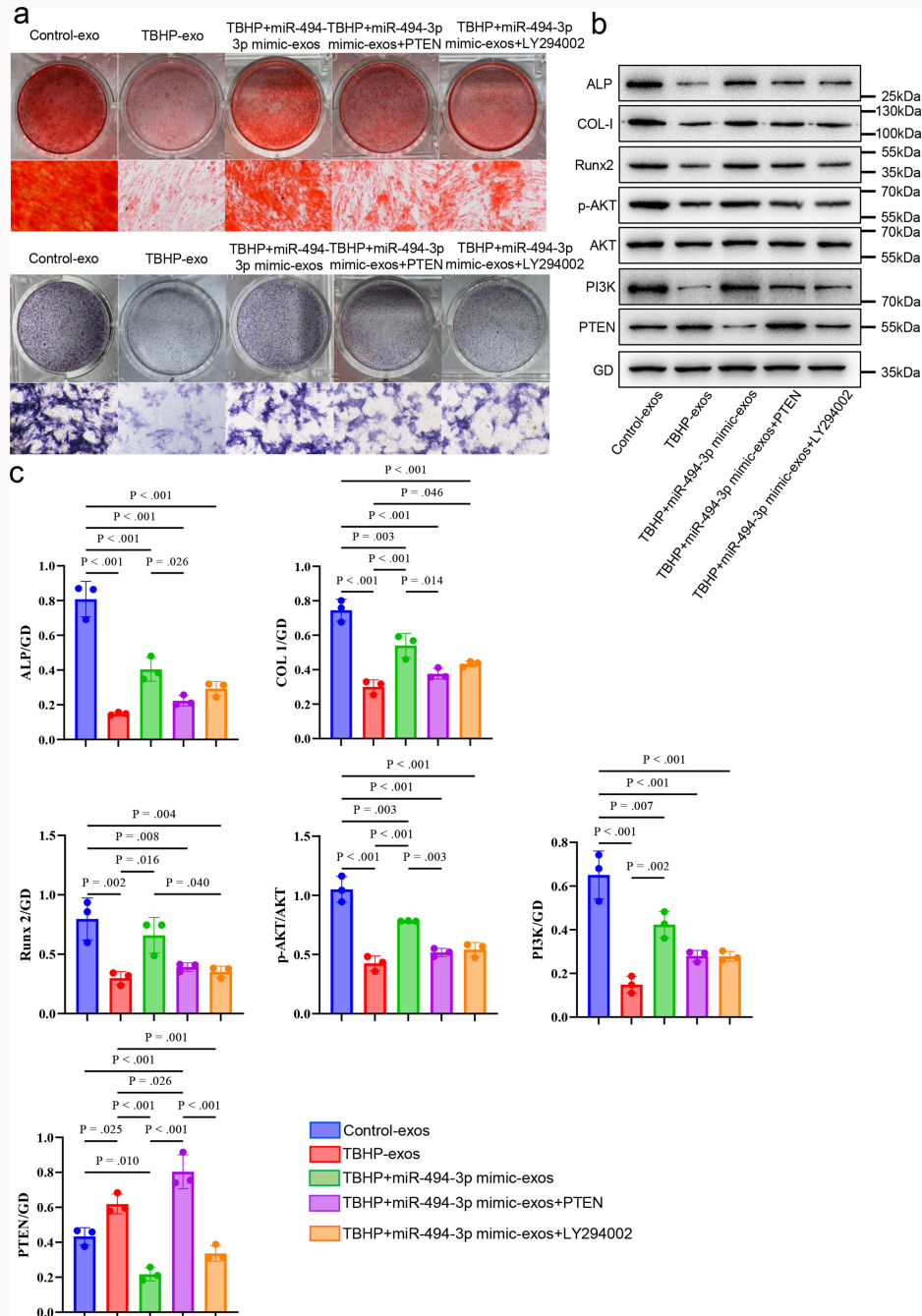
Fig. 3
miR-494-3p in MLO-Y4 cell-derived exosomes regulated osteogenic differentiation of MC3T3-E1 cells via the phosphatase and tensin homolog (PTEN)/phosphoinositide 3-kinase (PI3K)/AKT pathway. a) Alkaline phosphatase (ALP) and Alizarin Red S staining of MC3T3-E1 cells on day 21 in different treatment groups. The magnification is 10× (lower part). b) and c) Western blotting and grayscale analysis of ALP, Runt-related transcription factor 2 (Runx2), collagen type I α1 (Col-I), p-AKT, AKT, PI3K, and PTEN expression in MC3T3-E1 cells in different treatment groups. Data are shown as column charts and the p-values were calculated by one-way analysis of variance with Sidak's multiple comparison tests. The p-values were specified only when p < 0.05 (statistically significant). GD, glyceraldehyde 3-phosphate dehydrogenase; miR, microRNA; TBHP, tert-Butyl hydroperoxide.

are involved in multiple metabolic processes, but none of them has a proven role in regulating age-related bone loss. Among all the differentially expressed miRNAs, we selected miR-494-3p for further investigation, because it was the most strongly down-regulated miRNA in senescent MLO-Y4 cell-derived exosomes. RT-qPCR confirmed the findings of RNA sequencing (Supplementary Figure ed). Moreover, we also performed RT-qPCR to compare the change degrees for the expression levels of six main miRNAs based on RNA sequencing in exosomes derived from normal or senescent MLO-Y4 cells, which also confirmed that miR-494-3p was the miRNA with the most strongly changed expression (Supplementary Figure f). When senescent MLO-Y4 cells were transfected with miR-494-3p mimics, the expression of exosomal miR-494-3p was upregulated (Supplementary Figure ee). Additionally, ALP and Alizarin Red S staining of MC3T3-E1 cells indicated that inhibition of osteogenic differentiation by senescent MLO-Y4 cell-derived exosomes was reversed upon upregulation of miR-494-3p in exosomes derived from the senescent MLO-Y4 cells (Supplementary Figure g).
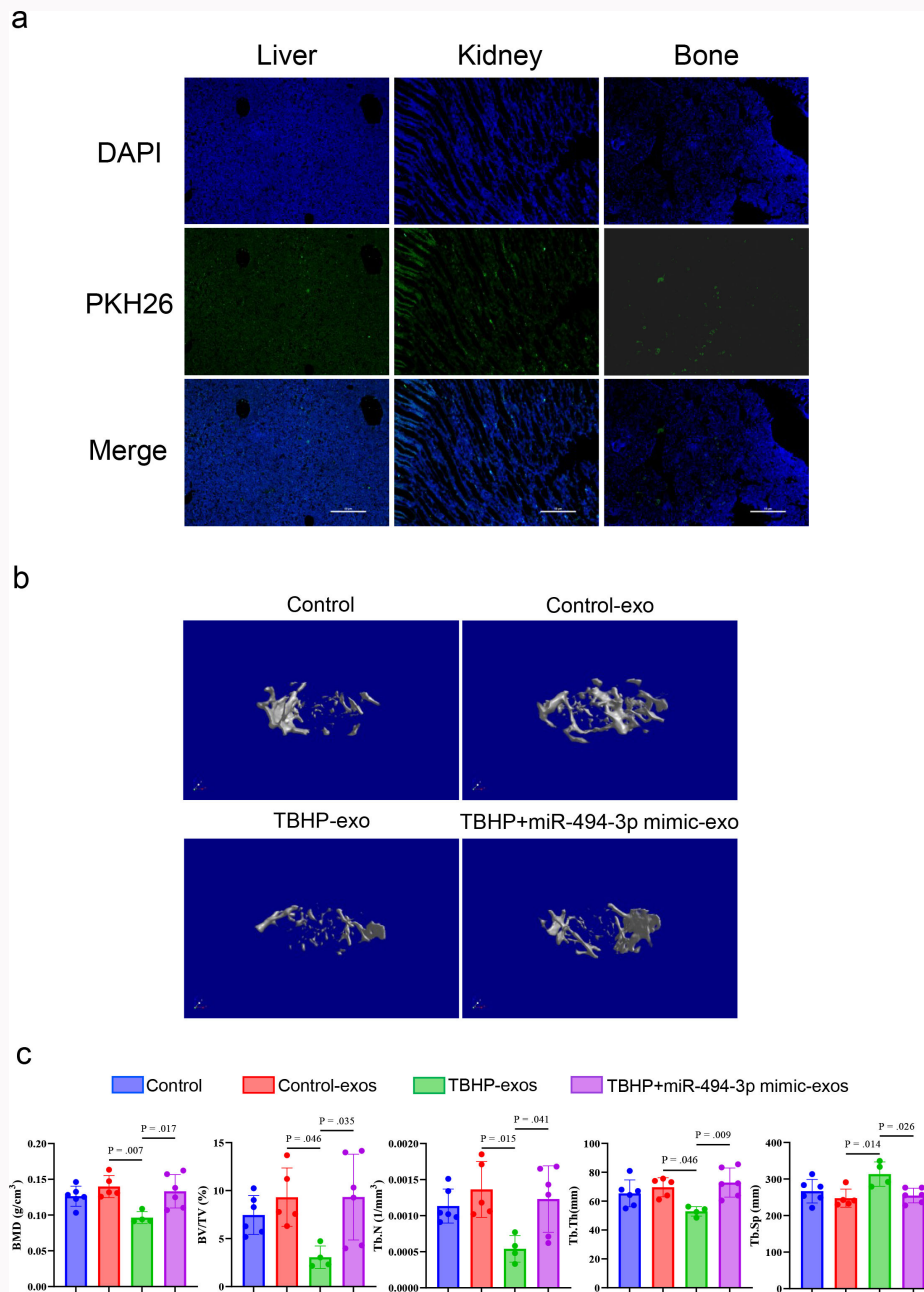
Down-expression of miR-494-3p in senescent osteocyte-derived exosomes inhibits osteogenesis and accelerates age-related bone loss via PTEN/PI3K/AKT pathway
C. Yao, J. Sun, W. Luo, et al

59

Fig. 4

Micro-CT of distal femoral metaphysis from SAMP6 mice treated with different exosomes. a) Fluorescence staining of organs to observe the distribution of injected exosomes. Scale bar = 50 μm and the magnification is 10×. b) Micro-CT 3D imaging of the distal femoral metaphysis. c) Microarchitecture parameters according to micro-CT. Data are shown as column charts and the p-values were calculated by one-way analysis of variance with Sidak's multiple comparison tests. The p-values were specified only when $p < 0.05$ (statistically significant). BMD, bone mineral density; BV, bone volume; DAPI, 4, 6-diamidino-2-phenylindole; miR, microRNA; TBHP, tert-Butyl hydroperoxide; Tb.N, trabecular number; Tb.Sp, trabecular separation; Tb.Th, trabecular thickness; TV, total volume.

miR-494-3p in MLO-Y4 cell-derived exosomes regulate osteogenic differentiation via the PTEN/PI3K/AKT pathway

KEGG pathway analysis showed that miR-494-3p is mainly involved in pathways related to mitogen-activated protein kinase (MAPK), cancer, PI3K-AKT, and metabolic processes (Supplementary Figure ec). The TargetScan database was used to predict the target genes of miR-494-3p, and the results predicted interaction of miR-494-3p with wild-type and mutant PTEN. The binding site for miR-494-3p in PTEN is shown in Supplementary Figure ef, and a luciferase reporter assay also demonstrated direct interaction between

miR-494-3p and PTEN. PTEN is a crucial negative regulator of the PI3K/AKT signalling pathway, and PI3K/AKT signalling has well-established roles in cell growth, differentiation, and metabolism.

The results presented in Figures 3a to 3c and Supplementary Figure h demonstrate the downstream signalling pathway of exosomal miR-494-3p in MC3T3-E1 cells. Western blotting and RT-qPCR showed that PTEN expression was upregulated and the PI3K/AKT pathway was inhibited in MC3T3E-1 cells treated with exosomes from senescent MLO-Y4 cells compared with the control group. When exosomal
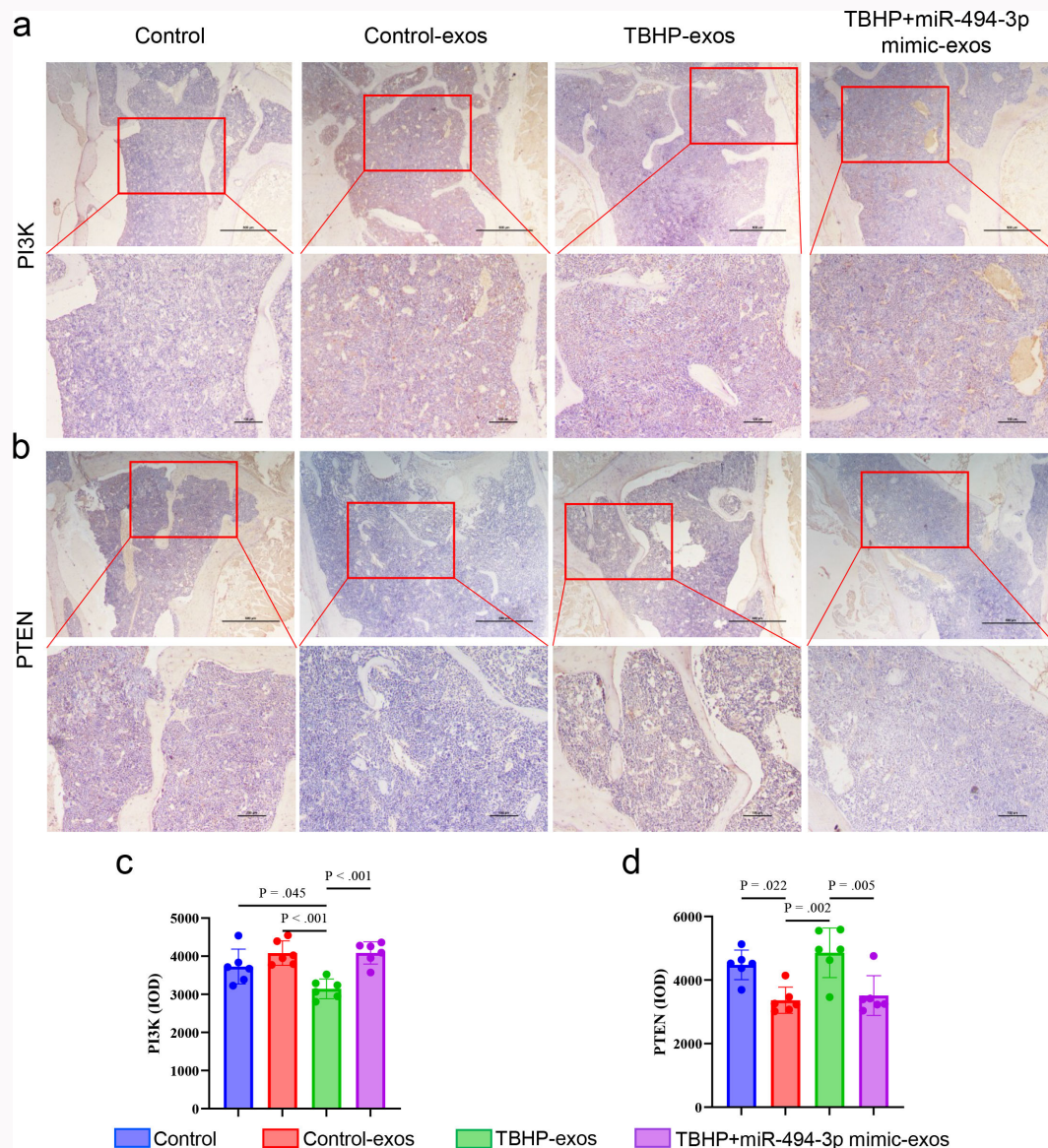
miR-494-3p was upregulated through mimics, PTEN expression was inhibited and PI3K/AKT signalling was increased in MC3T3E-1 cells. Moreover, plasmid transfection to upregulate PTEN rescued the osteogenic effect of exosomal miR-494-3p on MC3T3-E1 cells based on the results of ALP staining, Alizarin Red S staining, western blotting, and RT-qPCR, which suggests that exosomal miR-494-3p regulates MC3T3-E1 cells by inhibiting PTEN. In addition, overexpression of PTEN inhibited PI3K/AKT signalling. Treatment with the PI3K/AKT inhibitor LY294002 also rescued the effect of exosomal miR-494-3p on MC3T3-E1 cells. These experiments suggest that miR-494-3p in MLO-Y4 cell-derived exosomes regulates osteogenic differentiation of osteoblasts by targeting the PTEN/PI3K/AKT pathway.

Exosomal miR-494-3p regulates age-related bone loss in SAMP6 mice

SAMP6 mice were employed as an age-related osteoporosis model for in vivo experiments. Senescent MLO-Y4 cell-derived exosomes labelled with PKH26 were injected into the four-month-old mice intravenously into the tail vein. Fluorescence imaging showed that the exosomes accumulated in the liver, kidney, and bone tissue by three hours after injection (Figure 4a). At eight weeks after exosome injection, micro-CT 3D imaging of the distal femoral metaphysis showed accelerated bone loss in mice that received senescent MLO-Y4 cell-derived exosomes compared with the control mice and those that received normal exosomes (Figure 4b). Additionally, significant reductions in BMD, BV/TV, TB.N, and Tb.Th and a higher Tb.Sp were detected in the senescent exosome group

Down-expression of miR-494-3p in senescent osteocyte-derived exosomes inhibits osteogenesis and accelerates age-related bone loss via PTEN/PI3K/AKT pathway
C. Yao, J. Sun, W. Luo, et al

61

(Figure 4c). However, upregulation of exosomal miR-494-3p by mimics rescued these effects. Immunohistochemical staining for PI3K, PTEN, ALP, Runx2, and Col-I proteins revealed the effects of senescent MLO-Y4 cell-derived exosomes on osteogenesis and the relevant pathway in vivo, consistent with the results of in vitro experiments (Figure 5 and Supplementary Figure i).

Discussion

Cellular senescence plays a key role in the progression of multiple degenerative diseases, including senile osteoporosis. Promisingly, targeting cellular senescence can prevent age-related bone loss in mice.[28] Osteocytes constitute the great majority of cells in bone, and senescent osteocytes predominantly account for SASP, providing a new therapeutic paradigm. In the present study, we induced MLO-Y4 cell senescence through oxidative stress generated by TBHP treatment and isolated exosomes released by senescent MLO-Y4 cells. Our observations of exosomal uptake and differentiation by MC3T3-E1 cells after treatment with senescent MLO-Y4 cell-derived exosomes confirmed that senescent MLO-Y4 cell-derived exosomes inhibited osteogenic differentiation. Furthermore, we identified differentially expressed miRNAs between exosomes from senescent and normal MLO-Y4 cells via high-throughput RNA sequencing with RT-qPCR confirmation. This analysis revealed significantly lower expression of miR-494-3p in exosomes derived from senescent MLO-Y4 cells. After transfecting senescent MLO-Y4 cells with mimics to overexpress exosomal miR-494-3p, we observed that the effects of the exosomes on MC3T3-E1 cells were reversed or attenuated, suggesting that miR-494-3p is a key miRNA in the effects of the senescent cells. According to the TargetScan database and luciferase reporter assay, PTEN is the target gene of miR-494-3p, and miR-494-3p inhibits expression of PTEN in MC3T3-E1 cells. Moreover, our rescue experiments demonstrated the involvement of the PTEN/PI3K/Akt signalling pathway in the regulation of MC3T3-E1 cell differentiation by miR-494-3p. Our in vivo experiments in the SAMP6 mouse model showed that injection of exosomes with different levels of miR-494-3p via the tail veins affected bone mass and the expression of downstream pathway proteins. Together, the results of this study indicate that reduced expression of miR-494-3p in exosomes derived from senescent osteocytes interrupts bone homeostasis and influences age-related bone loss; an illustration of the proposed mechanism is presented in Supplementary Figure j.

Research has demonstrated that exosomes mediate intercellular communications between different bone cell types, and that these communications are important for the regulation of bone homeostasis.[31] Exosome production by MLO-Y4 cells and their inclusion of miRNA were reported in 2017,[35] which was later than similar findings for other bone cell types, and subsequent studies on osteocyte-derived exosomes have been relatively few. One study showed that myostatin-modified osteocyte-derived exosomes may regulate osteoblast differentiation through the miR-218/Wnt/β-catenin pathway.[36] Another study found that exosomes from osteocytes exposed to mechanical strain promote human periodontal ligament stem cell proliferation and osteogenic differentiation via the miR-181b-5p/PTEN/AKT axis.[37] Senescence of osteocytes and its influence on homeostasis and age-related bone loss have been confirmed.[28,38] However, whether exosomes from senescent osteocytes influence homeostasis and age-related bone loss, and the underlying mechanism, have not been explored. For the first time in this study, we demonstrated that senescent MLO-Y4 cell-derived exosomes inhibited bone formation and accelerated age-related bone loss in vitro and in vivo. Moreover, to explore the underlying molecular mechanism, we performed RNA sequencing to detect DEGs in exosomes from senescent cells. The results identified 35 miRNAs upregulated and 15 miRNAs downregulated in exosomes derived from senescent MLO-Y4 cells compared with exosomes derived from normal MLO-Y4 cells. While GO enrichment analysis indicated that differentially expressed miRNAs are involved in metabolic processes, none has been previously linked to age-related bone loss. Still, our results provide valuable insight regarding novel potential therapeutic targets for senile osteoporosis.

Among all the differentially expressed miRNAs, we selected miR-494-3p for further mechanistic studies. In previous research, miR-494-3p was mainly connected with proliferation, invasion, or migration of tumour cells, such as those in hepatocellular carcinoma, endometrial cancer, lung cancer, and others.[39-41] miR-494-3p was also shown to regulate the response to lipopolysaccharide-induced inflammation in RAW264.7 cells.[42] Another study found that miR-494-3p expression induced by compressive force inhibits the proliferation of MC3T3-E1 cells.[43] Here, we found that miR-494-3p expression was downregulated in exosomes derived from senescent MLO-Y4 cells to less than one-eighth of the level in exosomes from normal MLO-Y4 cells, which was confirmed by RT-qPCR. Our experiments in vitro and in the SAMP6 mouse model further demonstrated that miR-494-3p mediates the influence of MLO-Y4 cell-derived exosomes on MC3T3-E1 cells and age-related bone loss. The results of a luciferase reporter assay identified PTEN as the target gene of miR-494-3p, which is consistent with the results of previous research.[39,41,42] miR-494-3p may target some other genes, such as PGC1-α, FGFR2, CXCR4, ROCK1, or SOCS6, as some other studies have reported,[43-46] but these were not identified in our study.

Previous studies revealed that PTEN is targeted by several miRNAs and is mainly involved in tumorigenesis via the regulation of various cellular processes including cell cycle progression, proliferation, migration, and apoptosis.[47-49] Additional studies reported that PTEN may mediate the cellular inflammatory response.[42,50,51] It is well established that PTEN, as a lipid phosphatase, elicits these various biological functions mainly by inhibiting the downstream PI3K/AKT signalling pathway. In the present study, due to reduced expression of miR-494-3p in exosomes derived from senescent osteocytes, PTEN expression was upregulated in MC3T3-E1 cells upon uptake of those exosomes. Then, PI3K/AKT signalling was inhibited by increased PTEN expression, which influenced the functions of the osteoblasts. In SAMP6 mice, immunohistochemical staining for PI3K, PTEN, ALP, Runx2, and Col-I and bone mass quantification from micro-CT showed corresponding changes after injection of different exosomes. PI3K/AKT signalling is well known to be coupled with bone

metabolism and osteoporosis. Many studies have reported that activation of PI3K/AKT signalling promotes the differentiation and osteogenesis of osteoblasts,[52,53] which is consistent with our findings. In contrast, Yin et al[54] reported that miR-140-3p inhibits the proliferation and differentiation of C2C12 cells by targeting PTEN and activating the PI3K/AKT pathway. Li et al[55] also reported that miR-363-3p inhibits osteogenic differentiation by targeting the PTEN/PI3K/Akt pathway. Thus, the roles of the PTEN/PI3K/AKT pathway in bone metabolism and osteoporosis may be diverse, and further research is needed to gain a clearer understanding.

In the present study, we explored the regulation of osteogenic differentiation of MC3T3-E1 cells by osteocyte-derived exosomes. As signalling cells in bone, the regulatory functions and the underlying mechanism of osteocytes are complex and our understanding of them remains incomplete. In addition to osteoblasts, senescent osteocytes may also regulate the functions of BMSCs, mononuclear macrophages, and osteoclasts during progression of osteoporosis.[25-27] In addition to exosome release, senescent osteocytes may also function in other ways, such as producing inflammation or SASP.[14,27] These possibilities were not explored in our study. Instead of isolating primary cells from aged mice, we induced senescence in MLO-Y4 cells through application of oxidative stress for our experiments. Physiologically, ageing of cells is caused by multiple stimuli in addition to oxidative stress, which is much more complex than in in vitro experiments. Also, in addition to miR-494-3p, RNA sequencing detected many other differentially expressed miRNAs in exosomes derived from normal and senescent MLO-Y4 cells. These miRNAs, or other unknown proteins and lipids, may also play important biological roles in the progress of age-related osteoporosis, and thus further research is warranted.

For the in vivo rescue experiments, we performed micro-CT and only analyzed the cancellous bone to evaluate bone mass. Compared with cortical bone, the change of cancellous bone may reflect the degree or progress of osteoporosis more visually or directly, which we found were also applied alone in other published research.[56-58] Of course, cortical bone analysis would absolutely make the evaluation of bone mass fuller. Similarly, calcein labelling should also be considered in in vivo experiments, which is widely used to reflect bone formation dynamically. Moreover, only male mice were used in the in vivo experiments, to exclude the effects of oestrogen on bone loss in this study, however we believe that the senescence of osteocytes and intercellular communications mediated by exosomes also occur in female bodies, as these are common phenomena regardless of sex. Therefore, we believe that our research can be translated to females, which needs confirmation by further studies.

In conclusion, this study showed that senescent osteocyte-derived exosomes inhibited osteogenic differentiation of osteoblasts, and accelerated age-related bone loss in SAMP6 mice. These effects resulted from reduced expression of miR-494-3p in senescent osteocyte-derived exosomes, which targets the PTEN/PI3K/Akt axis. While specifically clearing senescent cells would be difficult to achieve in humans and likely to have adverse side effects, targeting the miR-494-3p/PTEN/PI3K/Akt axis identified in our study may represent a novel therapeutic strategy for preventing and treating impaired bone homeostasis, and age-related osteoporosis.

Supplementary material

The supplementary material section contains most of the reverse transcription-quantitative polymerase chain reaction results and a portion of the Alizarin Red S and alkaline phosphatase staining results. An ARRIVE checklist is also included to show that the ARRIVE guidelines were adhered to in this study.

References

1. **Compston JE**, **McClung MR**, **Leslie WD**. Osteoporosis. *Lancet*. 2019;393(10169):364–376.
2. **Rachner TD**, **Khosla S**, **Hofbauer LC**. Osteoporosis: now and the future. *Lancet*. 2011;377(9773):1276–1287.
3. **Shi N**, **Foley K**, **Lenhart G**, **Badamgarav E**. Direct healthcare costs of hip, vertebral, and non-hip, non-vertebral fractures. *Bone*. 2009;45(6):1084–1090.
4. **Khosla S**, **Hofbauer LC**. Osteoporosis treatment: recent developments and ongoing challenges. *Lancet Diabetes Endocrinol*. 2017;5(11):898–907.
5. **Reid IR**, **Billington EO**. Drug therapy for osteoporosis in older adults. *Lancet*. 2022;399(10329):1080–1092.
6. **Dong W**, **Postlethwaite BC**, **Wheller PA**, **et al**. Beta-caryophyllene prevents the defects in trabecular bone caused by Vitamin D deficiency through pathways instated by increased expression of klotho. *Bone Joint Res*. 2022;11(8):528–540.
7. **Johnston CB**, **Dagar M**. Osteoporosis in older adults. *Med Clin North Am*. 2020;104(5):873–884.
8. **Boonen S**, **Singer AJ**. Osteoporosis management: impact of fracture type on cost and quality of life in patients at risk for fracture I. *Curr Med Res Opin*. 2008;24(6):1781–1788.
9. **Kim J-M**, **Lin C**, **Stavre Z**, **Greenblatt MB**, **Shim J-H**. Osteoblast-osteoclast communication and bone homeostasis. *Cells*. 2020;9(9):2073.
10. **Maestro-Paramio L**, **García-Rey E**, **Bensiamar F**, **Saldaña L**. Osteoblast function in patients with idiopathic osteonecrosis of the femoral head: implications for a possible novel therapy. *Bone Joint Res*. 2021;10(9):619–628.
11. **Schlaff WD**. Introduction: an update on bone metabolism and osteoporosis. *Fertil Steril*. 2019;112(5):773–774.
12. **Grunewald M**, **Kumar S**, **Sharife H**, **et al**. Counteracting age-related VEGF signaling insufficiency promotes healthy aging and extends life span. *Science*. 2021;373(6554):eabc8479.
13. **Tu C**, **Lai S**, **Huang Z**, **et al**. Accumulation of advanced oxidation protein products contributes to age-related impairment of gap junction intercellular communication in osteocytes of male mice. *Bone Joint Res*. 2022;11(7):413–425.
14. **Wang Z**, **Zhang X**, **Cheng X**, **et al**. Inflammation produced by senescent osteocytes mediates age-related bone loss. *Front Immunol*. 2023;14:1114006.
15. **Abe S**, **Kashii M**, **Shimada T**, **et al**. Relationship between distal radius fracture severity and 25-hydroxyvitamin-D level among perimenopausal and postmenopausal women. *Bone Jt Open*. 2022;3(3):261–267.
16. **He S**, **Sharpless NE**. Senescence in health and disease. *Cell*. 2017;169(6):1000–1011.
17. **Zhang X**, **Habiballa L**, **Aversa Z**, **et al**. Characterization of cellular senescence in aging skeletal muscle. *Nat Aging*. 2022;2(7):601–615.
18. **Khosla S**, **Farr JN**, **Tchkonia T**, **Kirkland JL**. The role of cellular senescence in ageing and endocrine disease. *Nat Rev Endocrinol*. 2020;16(5):263–275.
19. **Jeon OH**, **Kim C**, **Laberge R-M**, **et al**. Local clearance of senescent cells attenuates the development of post-traumatic osteoarthritis and creates a pro-regenerative environment. *Nat Med*. 2017;23(6):775–781.
20. **Zong Z**, **Zhang X**, **Yang Z**, **et al**. Rejuvenated ageing mesenchymal stem cells by stepwise preconditioning ameliorates surgery-induced osteoarthritis in rabbits. *Bone Joint Res*. 2021;10(1):10–21.
21. **Khosla S**, **Farr JN**, **Kirkland JL**. Inhibiting cellular senescence: a new therapeutic paradigm for age-related osteoporosis. *J Clin Endocrinol Metab*. 2018;103(4):1282–1290.

Down-expression of miR-494-3p in senescent osteocyte-derived exosomes inhibits osteogenesis and accelerates age-related bone loss via PTEN/PI3K/AKT pathway
C. Yao, J. Sun, W. Luo, et al

63

22. **Farr JN**, **Kaur J**, **Doolittle ML**, **Khosla S**. Osteocyte cellular senescence. *Curr Osteoporos Rep*. 2020;18(5):559–567.

23. **Robling AG**, **Bonewald LF**. The osteocyte: new insights. *Annu Rev Physiol*. 2020;82:485–506.

24. **Li MCM**, **Chow SK-H**, **Wong RMY**, **et al**. Osteocyte-specific dentin matrix protein 1: the role of mineralization regulation in low-magnitude high-frequency vibration enhanced osteoporotic fracture healing. *Bone Joint Res*. 2022;11(7):465–476.

25. **Compton JT**, **Lee FY**. A review of osteocyte function and the emerging importance of sclerostin. *J Bone Joint Surg Am*. 2014;96-A(19):1659–1668.

26. **Plotkin LI**, **Bellido T**. Erratum: Osteocytic signalling pathways as therapeutic targets for bone fragility. *Nat Rev Endocrinol*. 2016;Epub ahead of print.

27. **Ding P**, **Gao C**, **Gao Y**, **et al**. Osteocytes regulate senescence of bone and bone marrow. *Elife*. 2022;11:e81480.

28. **Farr JN**, **Xu M**, **Weivoda MM**, **et al**. Corrigendum: Targeting cellular senescence prevents age-related bone loss in mice. *Nat Med*. 2017;23(11):1384.

29. **Geng Q**, **Gao H**, **Yang R**, **Guo K**, **Miao D**. Pyrroloquinoline quinone prevents estrogen deficiency-induced osteoporosis by inhibiting oxidative stress and osteocyte senescence. *Int J Biol Sci*. 2019;15(1):58–68.

30. **Kennedy OD**, **Herman BC**, **Laudier DM**, **Majeska RJ**, **Sun HB**, **Schaffler MB**. Activation of resorption in fatigue-loaded bone involves both apoptosis and active pro-osteoclastogenic signaling by distinct osteocyte populations. *Bone*. 2012;50(5):1115–1122.

31. **Gao M**, **Gao W**, **Papadimitriou JM**, **Zhang C**, **Gao J**, **Zheng M**. Exosomes-the enigmatic regulators of bone homeostasis. *Bone Res*. 2018;6:36.

32. **Xie X**, **Xiong Y**, **Panayi AC**, **et al**. Exosomes as a novel approach to reverse osteoporosis: a review of the literature. *Front Bioeng Biotechnol*. 2020;8:594247.

33. **Ge M**, **Ke R**, **Cai T**, **Yang J**, **Mu X**. Identification and proteomic analysis of osteoblast-derived exosomes. *Biochem Biophys Res Commun*. 2015;467(1):27–32.

34. **Li D**, **Liu J**, **Guo B**, **et al**. Osteoclast-derived exosomal miR-214-3p inhibits osteoblastic bone formation. *Nat Commun*. 2016;7:10872.

35. **Sato M**, **Suzuki T**, **Kawano M**, **Tamura M**. Circulating osteocyte-derived exosomes contain miRNAs which are enriched in exosomes from MLO-Y4 cells. *Biomed Rep*. 2017;6(2):223–231.

36. **Qin Y**, **Peng Y**, **Zhao W**, **et al**. Myostatin inhibits osteoblastic differentiation by suppressing osteocyte-derived exosomal microRNA-218: a novel mechanism in muscle-bone communication. *J Biol Chem*. 2017;292(26):11021–11033.

37. **Lv P-Y**, **Gao P-F**, **Tian G-J**, **et al**. Osteocyte-derived exosomes induced by mechanical strain promote human periodontal ligament stem cell proliferation and osteogenic differentiation via the miR-181b-5p/PTEN/AKT signaling pathway. *Stem Cell Res Ther*. 2020;11(1):295.

38. **Farr JN**, **Fraser DG**, **Wang H**, **et al**. Identification of senescent cells in the bone microenvironment. *J Bone Miner Res*. 2016;31(11):1920–1929.

39. **Zhu L**, **Wang X**, **Wang T**, **Zhu W**, **Zhou X**. miR-494-3p promotes the progression of endometrial cancer by regulating the PTEN/PI3K/AKT pathway. *Mol Med Rep*. 2019;19(1):581–588.

40. **Faversani A**, **Amatori S**, **Augello C**, **et al**. miR-494-3p is a novel tumor driver of lung carcinogenesis. *Oncotarget*. 2017;8(5):7231–7247.

41. **Lin H**, **Huang Z-P**, **Liu J**, **et al**. MiR-494-3p promotes PI3K/AKT pathway hyperactivation and human hepatocellular carcinoma progression by targeting PTEN. *Sci Rep*. 2018;8(1):10461.

42. **Zhang S**, **He K**, **Zhou W**, **Cao J**, **Jin Z**. miR-494-3p regulates lipopolysaccharide-induced inflammatory responses in RAW264.7 cells by targeting PTEN. *Mol Med Rep*. 2019;19(5):4288–4296.

43. **Iwawaki Y**, **Mizusawa N**, **Iwata T**, **et al**. MiR-494-3p induced by compressive force inhibits cell proliferation in MC3T3-E1 cells. *J Biosci Bioeng*. 2015;120(4):456–462.

44. **Lemecha M**, **Morino K**, **Imamura T**, **et al**. MiR-494-3p regulates mitochondrial biogenesis and thermogenesis through PGC1-α signalling in beige adipocytes. *Sci Rep*. 2018;8(1):15096.

45. **Rontauroli S**, **Norfo R**, **Pennucci V**, **et al**. miR-494-3p overexpression promotes megakaryocytopoiesis in primary myelofibrosis hematopoietic stem/progenitor cells by targeting SOCS6. *Oncotarget*. 2017;8(13):21380–21397.

46. **Pazzaglia L**, **Pollino S**, **Vitale M**, **et al**. miR-494.3p expression in synovial sarcoma: role of CXCR4 as a potential target gene. *Int J Oncol*. 2019;54(1):361–369.

47. **Stambolic V**, **Suzuki A**, **de la Pompa JL**, **et al**. Negative regulation of PKB/Akt-dependent cell survival by the tumor suppressor PTEN. *Cell*. 1998;95(1):29–39.

48. **Chen C-Y**, **Chen J**, **He L**, **Stiles BL**. PTEN: tumor suppressor and metabolic regulator. *Front Endocrinol (Lausanne)*. 2018;9:338.

49. **Ghafouri-Fard S**, **Abak A**, **Shoorei H**, **et al**. Regulatory role of microRNAs on PTEN signaling. *Biomed Pharmacother*. 2021;133:110986.

50. **Cao X**, **Wei G**, **Fang H**, **et al**. The inositol 3-phosphatase PTEN negatively regulates Fc gamma receptor signaling, but supports Toll-like receptor 4 signaling in murine peritoneal macrophages. *J Immunol*. 2004;172(8):4851–4857.

51. **Zheng C**, **Tang F**, **Min L**, **Hornicek F**, **Duan Z**, **Tu C**. PTEN in osteosarcoma: recent advances and the therapeutic potential. *Biochim Biophys Acta Rev Cancer*. 2020;1874(2):188405.

52. **Li H**, **Li T**, **Fan J**, **et al**. miR-216a rescues dexamethasone suppression of osteogenesis, promotes osteoblast differentiation and enhances bone formation, by regulating c-Cbl-mediated PI3K/AKT pathway. *Cell Death Differ*. 2015;22(12):1935–1945.

53. **Zhan J**, **Yan Z**, **Zhao M**, **et al**. Allicin inhibits osteoblast apoptosis and steroid-induced necrosis of femoral head progression by activating the PI3K/AKT pathway. *Food Funct*. 2020;11(9):7830–7841.

54. **Yin R**, **Jiang J**, **Deng H**, **Wang Z**, **Gu R**, **Wang F**. miR-140-3p aggregates osteoporosis by targeting PTEN and activating PTEN/PI3K/AKT signaling pathway. *Hum Cell*. 2020;33(3):569–581.

55. **Li M**, **Luo R**, **Yang W**, **Zhou Z**, **Li C**. miR-363-3p is activated by MYB and regulates osteoporosis pathogenesis via PTEN/PI3K/AKT signaling pathway. *In Vitro Cell Dev Biol Anim*. 2019;55(5):376–386.

56. **Zhou X**, **Sun S**, **Chen Y**, **et al**. Pulsed frequency modulated ultrasound promotes therapeutic effects of osteoporosis induced by ovarian failure in mice. *Ultrasonics*. 2023;132:106973.

57. **Wang L**, **Pan Y**, **Liu M**, **et al**. Wen-Shen-Tong-Luo-Zhi-Tong Decoction regulates bone-fat balance in osteoporosis by adipocyte-derived exosomes. *Pharm Biol*. 2023;61(1):568–580.

58. **Tao Z-S**, **Zhou W-S**, **Xu H-G**, **Yang M**. Parathyroid hormone (1-34) can reverse the negative effect of valproic acid on the osseointegration of titanium rods in ovariectomized rats. *J Orthop Translat*. 2021;27:67–76.

Author information

C. Yao, PhD, Orthopaedic Surgeon
J. Sun, PhD, Orthopaedic Surgeon
W. Luo, MS, Orthopaedic Surgeon
H. Chen, MS, Orthopaedic Surgeon
T. Chen, MS, Orthopaedic Surgeon
C. Chen, MS, Orthopaedic Surgeon
B. Zhang, PhD, Orthopaedic Surgeon
Y. Zhang, PhD, MD, Head of Department
Department of Orthopaedics, Affiliated Hospital of Nantong University, Medical School of Nantong University, Nantong, Jiangsu, China.

C. Yao, J. Sun, and W. Luo contributed equally to this work.

Ethical review statement

The overall animal experimental designs and schemes were approved by the Institutional Animal Care and Use Committee (IACUC) of the Medical School of Nantong University (No. S20220208004).

Open access funding

The authors report that the open access funding for their manuscript was self-funded.

Down-expression of miR-494-3p in senescent osteocyte-derived exosomes inhibits osteogenesis and accelerates age-related bone loss via PTEN/PI3K/AKT pathway
C. Yao, J. Sun, W. Luo, et al

65